



Nuclear spin-lattice relaxation time measurement in  $\text{NaD}_3(\text{SeO}_3)_2$   
by Roy Reinhart Knispel

A thesis submitted to the Graduate Faculty in partial fulfillment of the requirements for the degree of  
DOCTOR OF PHILOSOPHY in Physics  
Montana State University  
© Copyright by Roy Reinhart Knispel (1969)

Abstract:

Nuclear magnetic resonance and electrical conductivity-measurements were used to study the motions of hydrogen nuclei in deuterated sodium trihydrogen selenite crystals.

From electrical conductivity measurements, deuteron spin-lattice relaxation time measurements and direct deuteron interbond jump time measurements, an activation energy of  $0.73 \pm 0.07$  eV for deuteron interbond jumping was obtained. This motion provides the dominant contribution to the spin-lattice relaxation time above  $40^\circ\text{C}$ . In the temperature region from about  $10^\circ\text{C}$  to the ferroelectric transition temperature ( $-25^\circ\text{C}$  to  $-35^\circ\text{C}$  in the crystals studied) a high frequency motion, such as deuteron intrabond motion, was found to dominate the spin-lattice relaxation process.

The activation energy for this motion was found to be  $0.055 \pm 0.01$  eV. Below the ferroelectric transition, the deuteron spin-lattice relaxation time was found to be too short to be due to spin diffusion to paramagnetic impurities. This implied the presence of some molecular motion in which the deuterons are involved below the transition temperature, and a possible explanation was found in considering the contribution of torsional oscillations of  $\text{SeO}_3$  groups to the spin-lattice relaxation time of the deuterons. The temperature and frequency dependence of the spin-lattice relaxation time of  $\text{Na}^{23}$  nuclei were similar to those of the deuterons over the same temperature and frequency ranges. The possibility of deuteron motion contributing to  $\text{Na}^{23}$  relaxation was therefore considered. In the  $30^\circ\text{C}$  to  $80^\circ\text{C}$  range, where deuteron interbond jumping is the dominant deuteron relaxation mechanism, it was found that the  $\text{Na}^{23}$  relaxation showed too small an activation energy (0.35 eV) to arise from deuteron interbond jumping. The indication of deuteron intrabond motion in the paraelectric phase is indicative of a dynamic order-disorder type ferroelectric phase transition. Evidence that the transition is not exclusively of this type, however, was found in the fact that the suppression of intrabond motion with the onset of polarization cannot explain the decrease in the deuteron spin-lattice relaxation time observed in the temperature region below the transition.

NUCLEAR SPIN-LATTICE RELAXATION TIME MEASUREMENTS

IN  $\text{NaD}_3(\text{SeO}_3)_2$

by

ROY REINHART KNISPEL

A thesis submitted to the Graduate Faculty in partial fulfillment of the requirements for the degree

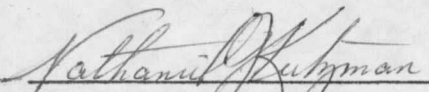
of

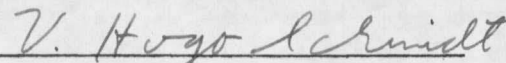
DOCTOR OF PHILOSOPHY

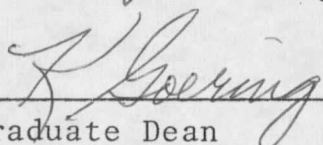
in

Physics

Approved:

  
Head, Major Department, *Acting*

  
Chairman, Examining Committee

  
Graduate Dean

MONTANA STATE UNIVERSITY  
Bozeman, Montana

December, 1969

## ACKNOWLEDGEMENTS

The author wishes to thank the National Aeronautics and Space Administration and the National Science Foundation for financial assistance and the National Institutes of Health for providing much of the material and equipment used in this research. To his advisor, Dr. V. Hugo Schmidt, he is especially grateful for constant encouragement and helpful discussion. He thanks F. L. Howell for stimulating discussion and help with the experimentation. To Robert Parker he extends appreciation both for many useful suggestions, and for his efforts in building the NMR pulse equipment which was used in much of this work. Helpful discussions with Drs. D. H. Dickey, Z. Trontelj, and J. A. Ball are also acknowledged. Thanks are extended to Fred Blankenburg for much help with the electronic equipment and to Harlan Wilhelm and Cecil Badgley for assistance with the machine work. Drs. Caughlan, Emerson, Jennings and Craig have been most willing to offer their assistance and the use of the facilities of the chemistry department. The writer extends his deep appreciation to his wife for her steady encouragement throughout this program, and thanks her for drawing the diagrams and typing the manuscript of this thesis.

## TABLE OF CONTENTS

Chapter		Page
	LIST OF TABLES . . . . .	vi
	LIST OF FIGURES . . . . .	vii
	ABSTRACT . . . . .	ix
I	INTRODUCTION . . . . .	1
II	KNOWN PROPERTIES OF STSe AND DSTSe . . . . .	5
III	NMR SPECTRA IN STSe AND DSTSe . . . . .	20
IV	DEUTERON MOTION ABOVE $T_c$ . . . . .	37
	Section I Electrical Conductivity . . . . .	37
	Section II Spin-lattice Relaxation Time of Deuterons . . . . .	40
	Section III Deuteron Interbond Jump Time . . . . .	57
	Section IV Sodium Relaxation Time . . . . .	65
V	SPIN-LATTICE RELAXATION TIME MEASUREMENTS BELOW $T_c$ . . . . .	77
VI	DISCUSSION OF RESULTS . . . . .	91
VII	EXPERIMENTAL TECHNIQUES AND APPARATUS . . . . .	97
	Section I Preparation of Samples . . . . .	97
	Section II Electrical Conductivity . . . . .	98
	Section III Continuous Wave (CW) Spectrometer . . . . .	104
	Section IV Pulse Spectrometer . . . . .	110
	Section V CW $T_1$ Measurement Technique . . . . .	115
	APPENDIX . . . . .	116
	Appendix A Contribution of Spin Diffusion to Paramagnetic Impurities to the Spin-lattice Relaxation Time . . . . .	117
	Appendix B Spin-lattice Relaxation via Quadrupolar Interaction . . . . .	121

Appendix C	Calculation of Autocorrelation Function for Deuteron Interbond Jumping . . . . .	125
Appendix D	Spectral Density for Na <sup>23</sup> Relaxation Due to Deuteron Interbond Motion	127
Appendix E	Least Squares Best Fit of T <sub>1</sub> Data .	130
LITERATURE CITED	. . . . .	136

## LIST OF TABLES

Table		Page
I	Cell Properties of $\text{NaH}_3(\text{SeO}_3)_2$ . . . . .	6
II	Atomic Coordinates . . . . .	7
III	Bond Properties (Paraelectric Phase) . . . . .	8
IV	Some Ferroelectric Properties of Alkali and Ammonium Trihydrogen Selenites . . . . .	16
V	Transition Energies and Entropy Changes in Phase Transitions of $\text{NaH}_3(\text{SeO}_3)_2$ and $\text{NaD}_3(\text{SeO}_3)_2$ . . . . .	18
VI	Electric Field Gradient Components of Deuteron Bonds in DSTSe at $25^\circ\text{C}$ . . . . .	28
VII	Possible Arrangements of $\text{HSeO}_3^-$ and $\text{H}_2\text{SeO}_3$ Groups . . . . .	34
VIII	Effective Ionic Charges for Fitting $\text{Na}^{23}$ EFG Tensor in STSe . . . . .	36
IX	Electrical Conductivity Above $T_c$ . . . . .	38
X	Electrical Conductivity Below $T_c$ . . . . .	39
XI	Activation Energies from Deuteron $T_1$ Measurements . . . . .	50
XII	EFG Tensor Components in Crystal System . . . . .	52
XIII	Crystals Used for Sodium $T_1$ Measurements . . . . .	65
XIV	Activation Energies from $\text{Na}^{23}$ $T_1$ Measurements . . . . .	72

## LIST OF FIGURES

Figure		Page
1	SeO <sub>3</sub> Pyramid in NaH <sub>3</sub> (SeO <sub>3</sub> ) <sub>2</sub> . . . . .	7
2	a, c Projection of Unit Cell of NaH <sub>3</sub> (SeO <sub>3</sub> ) <sub>2</sub>	9
3.	a, b Projection of Four Unit Cells of NaH <sub>3</sub> (SeO <sub>3</sub> ) <sub>2</sub> . . . . .	10
4.	Na(H <sub>(1-x)D<sub>x</sub></sub> ) <sub>3</sub> (SeO <sub>3</sub> ) <sub>2</sub> Phase Diagram . . . . .	13
5.	Na(H <sub>(1-x)D<sub>x</sub></sub> ) <sub>3</sub> (SeO <sub>3</sub> ) <sub>2</sub> Phase Diagram . . . . .	13
6.	Splitting of Nuclear Zeeman Levels by the Electric Quadrupolar Interaction for I=1	23
7.	Relationship of Rotation Axes to Crystalline Axes . . . . .	25
8.	Quadrupolar Splitting of Zeeman Levels of N Bonds . . . . .	26
9.	Quadrupolar Splitting of Zeeman Levels of S Bonds . . . . .	27
10.	NaD <sub>3</sub> (SeO <sub>3</sub> ) <sub>2</sub> Deuteron Quadrupole Perturbed NMR	30
11.	Simplified Notation for HSeO <sub>3</sub> <sup>-</sup> and H <sub>2</sub> SeO <sub>3</sub> Groups . . . . .	33
12.	a, b Projection of a Unit Cell of Ferroelectric NaD <sub>3</sub> (SeO <sub>3</sub> ) <sub>2</sub> . . . . .	35
13.	Deuteron T <sub>1</sub> Measurements . . . . .	44
14.	Deuteron T <sub>1</sub> Measurements . . . . .	45
15.	Deuteron T <sub>1</sub> Measurements . . . . .	46
16.	Orientalional Dependence of Interbond Jumping Contribution to W <sub>1</sub> and W <sub>2</sub> . . . . .	54
17.	Effect of Three 90° Pulses on Populations	58

## LIST OF FIGURES

18.	Example of Jump Time Measurement Data . . . . .	60
19.	Temperature Dependence of Deuteron Jump Time . . . . .	61
20.	$\text{Na}^{23}$ $T_1$ Measurements Above $T_c$ . . . . .	67
21.	Orientalional Dependence of $\text{Na}^{23}$ $T_1$ at 8 MHz . . . . .	68
22.	$\text{Na}^{23}$ $T_1$ Measurements at 14 MHz . . . . .	69
23.	$\text{Na}^{23}$ $T_1$ Measurements at 8 MHz . . . . .	70
24.	High Temperature Mechanism Contribution to $1/T_1$ . . . . .	71
25.	Deuteron $T_1$ Below $T_c$ and Proton $T_1$ . . . . .	78
26.	$\text{Na}^{23}$ $T_1$ Below $T_c$ . . . . .	80
27.	D $T_1$ Data Compared to $J(\omega) \propto (1 - p^2)$ . . . . .	83
28.	Log-log Plot of Reciprocal of $T_1$ vs Temperature . . . . .	87
29.	Deuteron $T_1$ Data Compared to Torsional Oscillation Theory Contributions . . . . .	90
30.	Conductivity Apparatus . . . . .	99
31.	Detail of Crystal Holder for Conductivity . . . . .	101
32.	Temperature Control for Robinson Spectrometer . . . . .	106
33.	Low-Temperature Device for Robinson Spectrometer . . . . .	108
34.	Temperature Control Apparatus . . . . .	109
35.	NMR Pulse Apparatus . . . . .	111
36.	Pulse Head . . . . .	112
37.	Detail of Gas Flow Inlets of Pulse Head . . . . .	113



## ABSTRACT

Nuclear magnetic resonance and electrical conductivity measurements were used to study the motions of hydrogen nuclei in deuterated sodium trihydrogen selenite crystals. From electrical conductivity measurements, deuteron spin-lattice relaxation time measurements and direct deuteron interbond jump time measurements, an activation energy of  $0.73 \pm 0.07$  eV for deuteron interbond jumping was obtained. This motion provides the dominant contribution to the spin-lattice relaxation time above  $40^\circ\text{C}$ . In the temperature region from about  $10^\circ\text{C}$  to the ferroelectric transition temperature ( $-25^\circ\text{C}$  to  $-35^\circ\text{C}$  in the crystals studied) a high frequency motion, such as deuteron intrabond motion, was found to dominate the spin-lattice relaxation process. The activation energy for this motion was found to be  $0.055 \pm 0.01$  eV. Below the ferroelectric transition, the deuteron spin-lattice relaxation time was found to be too short to be due to spin diffusion to paramagnetic impurities. This implied the presence of some molecular motion in which the deuterons are involved below the transition temperature, and a possible explanation was found in considering the contribution of torsional oscillations of  $\text{SeO}_3$  groups to the spin-lattice relaxation time of the deuterons. The temperature and frequency dependence of the spin-lattice relaxation time of  $\text{Na}^{23}$  nuclei were similar to those of the deuterons over the same temperature and frequency ranges. The possibility of deuteron motion contributing to  $\text{Na}^{23}$  relaxation was therefore considered. In the  $30^\circ\text{C}$  to  $80^\circ\text{C}$  range, where deuteron interbond jumping is the dominant deuteron relaxation mechanism, it was found that the  $\text{Na}^{23}$  relaxation showed too small an activation energy (0.35 eV) to arise from deuteron interbond jumping. The indication of deuteron intrabond motion in the paraelectric phase is indicative of a dynamic order-disorder type ferroelectric phase transition. Evidence that the transition is not exclusively of this type, however, was found in the fact that the suppression of intrabond motion with the onset of polarization cannot explain the decrease in the deuteron spin-lattice relaxation time observed in the temperature region below the transition.

## CHAPTER I: INTRODUCTION

The alkali trihydrogen selenite crystals are primarily of interest because of their dielectric properties.<sup>(1)</sup> Of the crystals in this family, the ferroelectric properties of sodium trihydrogen selenite ( $\text{NaH}_3(\text{SeO}_3)_2$  hereafter abbreviated STSe) and the contrasting properties of the deuterated analogue of this crystal ( $\text{NaD}_3(\text{SeO}_3)_2$  or DSTSe) are most unusual. At  $-79^\circ\text{C}$ , STSe undergoes a transition of second order from its paraelectric  $\alpha$  phase to a ferroelectric  $\beta$  phase.<sup>(2)</sup> At  $-172.5^\circ\text{C}$ , STSe exhibits another phase transition<sup>(3)</sup> to a second ferroelectric  $\gamma$  phase. This transition exhibits a thermal hysteresis of  $10.5^\circ\text{C}$  and is therefore of first order. The paraelectric  $\alpha$  phases of STSe and DSTSe are isomorphic but DSTSe exhibits only one phase transition, at  $-2.5^\circ\text{C}$ ,<sup>(4)</sup> to a ferroelectric phase<sup>(5,6)</sup> which is apparently<sup>(7)</sup> isomorphic to the lower ferroelectric  $\gamma$  phase of STSe. In DSTSe, there is no phase analogous to the  $\beta$  phase of STSe. These crystals are hydrogen-bonded, and the important changes in properties upon deuteration imply that the hydrogen-bonding plays an important role in the ferroelectric behavior.

Nuclear magnetic resonance (NMR) techniques have

proved useful in determining the electrical environment of nuclei with electric quadrupolar moments, and in detecting motions executed by various nuclei. The electric field gradients in a hydrogen bond can be studied by measuring the splitting of the deuteron Zeeman levels by the interaction of the deuteron's electric quadrupolar moment with the electric field gradient tensor. Changes in the electric environment of deuterons, and other nuclei with quadrupolar moments, such as  $\text{Na}^{23}$ , caused by ferroelectric phase changes, can be detected from NMR spectra of these nuclei. Furthermore, motions of nuclei, such as hindered rotations of molecular groups, single deuteron interbond and intrabond jumps, and random fluctuations of lattice modes of vibration may cause changes of magnetic fields or electric field gradients of the proper frequency to cause nuclear relaxation. Nuclear spin-lattice relaxation time measurements therefore provide a means of studying nuclear motions in crystals. For nuclei with  $I > \frac{1}{2}$ , an electric quadrupolar interaction is usually more effective in causing nuclear relaxation than is a magnetic dipolar interaction.

It was the intent of this investigation to study the environment and motions of hydrogens in a hydrogen-bonded material by NMR techniques. Sodium trihydrogen selenite

was chosen because of the possibility that some of the motions which might be detected could be related to the important ferroelectric properties of this material. Deuterated crystals were used because of the possibilities of additional information obtainable from interactions with the deuteron quadrupolar moment. Various experiments (to be discussed in the next chapter) have indicated that the phase transitions in STSe and DSTSe involve both ordering of the hydrogens and atomic displacement. Measurements of the NMR spectra of various nuclei ( $H^1$ ,  $H^2$ ,  $Na^{23}$ ) in these crystals have been reported (8,9,10,11) and will be discussed in Chapter III. These studies provided additional clear evidence for the presence of both elements in the nature of the transitions. This investigation deals primarily with spin-lattice relaxation time ( $T_1$ ) measurements and measurements intended to clarify the interpretation of the deuteron  $T_1$  measurements, which are discussed in Chapters IV and V. They reflect the presence of deuteron interbond and intrabond motion in the temperature range between the melting point and the ferroelectric transition. Below the transition, no effects of interbond motion are observed, and the dominant mechanism for deuteron spin relaxation seems

to arise from lattice vibration fluctuations and/or  $\text{SeO}_3$  motion rather than single particle (deuteron) motions. This does not mean that all deuteron motion stops below  $T_c$ , but it indicates that other motions become more important than individual deuteron motions in causing spin-lattice relaxation below the phase transition temperature.

## CHAPTER II: KNOWN PROPERTIES OF STSe and DSTSe

Three x-ray investigations of the crystal structure of STSe in the paraelectric phase have been made. (3,11,12) Unterleitner claims that the space group of this phase is  $P2_1/a$ , class  $2/m$ , while Chou and Tang\* claim that the Na and Se atoms conform to space group  $P2_1/a$  but to include the oxygens, the space group  $Pn$ , class  $m$ , is applicable. In  $P2_1/a$ , all  $SeO_3$  are related by the symmetry operations of the space group, while they are not in  $Pn$ . (For comparison,  $LiH_3(SeO_3)_2$  is of class  $m$ , and two types of  $SeO_3$  groups have been identified by Pepinsky and Vedam<sup>(2)</sup> in this crystal.) Detailed structural analyses of the lower temperature phases to locate all atomic positions have not been made on STSe, but approximate cell dimensions and symmetries have been determined. These results, based primarily on Unterleitner's work\*\*, are summarized in Tables I and II. To date, no structure studies have been done on either phase of DSTSe, but the paraelectric phase is

---

\* This translation of Ref. 11 is from Roger P. Kohin, Clark University, Worcester, Mass.

\*\* Anderson(9) found that these results were more consistent with the directions of O—H...O bonds implied by his efg tensor measurements of deuteron sites than the results of Chou and Tang.

TABLE I: CELL PROPERTIES OF  $\text{NaH}_3(\text{SeO}_3)_2$

	Paraelectric Phase $T > -79^\circ\text{C}$	Ferroelectric Phase I $-79^\circ\text{C}$ to $-172^\circ\text{C}$	Ferroelectric Phase II $T < -172^\circ\text{C}$
Crystal Symmetry	Monoclinic 2/m	Triclinic 1	Monoclinic m
Space Group	$P 2_1/c$	C	
a cell dimension	$10.36 \text{ \AA}$	$20.60 \text{ \AA}$	$10.4 \text{ \AA}$
b cell dimension	$4.84 \text{ \AA}$	$9.57 \text{ \AA}$	$9.57 \text{ \AA}$
c cell dimension	$5.80 \text{ \AA}$	$5.76 \text{ \AA}$	$5.75 \text{ \AA}$
Cell angle	$90^\circ$	$89^\circ 36'$	$90^\circ$
Cell angle	$91^\circ 10'$	$91^\circ$	
Cell angle	$90^\circ$	$90^\circ 18'$	$90^\circ$

TABLE II: ATOMIC COORDINATES

(Dimensions in Fractions of Unit Cell Dimensions)

Atom	x	y	z
Na	0.0	0.0	0.500
Se	0.170	0.380	0.0
O <sub>I</sub>	0.051	0.159	0.860
O <sub>II</sub>	0.145	0.281	0.290
O <sub>III</sub>	0.301	0.185	0.951

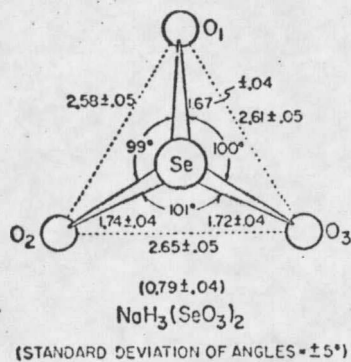


Figure 1:  $\text{SeO}_3$  Pyramid in  $\text{NaH}_3(\text{SeO}_3)_2$   
 (after Vedam, Okaya, & Pepinsky<sup>(2)</sup>)



assumed to have the same symmetry, space group, and interatomic distances as the  $\alpha$  phase of STSe. Most evidence indicates that the structure of the lower temperature phase of DSTSe is similar to that of the  $\gamma$  phase of STSe.

Figures 2 and 3 illustrate the hydrogen-bonding of the crystal. Of the three hydrogen bonds per molecule, two (N and N', Fig. 2 - length  $2.56 \text{ \AA}$ ) are identical. This is not evident from the figure but is from the x-ray studies and NMR spectra. The third bond (S - length  $2.61 \text{ \AA}$ ) is special in that its center is also a center of symmetry in the unit cell. We therefore use the following designations in referring to the two types of bonds:

TABLE III: BOND PROPERTIES (PARAELECTRIC PHASE)

length, $\text{\AA}$	designation	number/cell
2.56	N (non-symmetric)	4
2.61	S (symmetric)	2

From Fig. 3, it is evident that there are physically two types of N bonds and two types of S bonds, each having different directions. From x-ray studies by Pepinsky,<sup>(2)</sup> or from the atomic coordinates listed in Table 2, the dimensions of the  $\text{SeO}_3$  pyramid are obtained. Fig. 1 summarizes these interatomic parameters.







































































































































































































































































































